

# Comparison of an integral equation on energy and the ray-tracing technique in room acoustics

A. Le Bot<sup>a)</sup> and A. Bocquillet

*Laboratoire de Tribologie et Dynamique des Systèmes—UMR 5513 CNRS, École Centrale de Lyon, 36, Avenue Guy de Collongue 69131 BP163 Ecully, France*

(Received 31 May 1999; revised 12 December 1999; revised 5 May 2000; accepted 5 June 2000)

This paper deals with a comparison of two room acoustic models. The first one is an integral formulation stemming from power balance and the second is the ray-tracing technique with a perfectly diffuse reflection law. The common assumptions to both models are the uncorrelated wave hypothesis and the perfectly diffuse reflection law. The latter allows the use of these methods for nondiffuse fields beyond the validity domain of Sabine's formula. Comparisons of numerical simulations performed with the softwares RAYON and CeReS point out that these results are close to each other and finally, a formal proof is proposed showing that both methods are actually equivalent. © 2000 Acoustical Society of America. [S0001-4966(00)02309-2]

PACS numbers: 43.55.Ka, 43.55.Br, 43.50.Jh [JDQ]

## INTRODUCTION

The high-frequency range in acoustics and structural vibrations is often considered with the help of two simplifying assumptions. The first consists of neglecting the effects of interference. As an immediate consequence, energies of traveling waves can be added. This fact explains why energy quantities are more often used as the primary variables of high-frequency models instead of kinetic variables. Justifications for this assumption are numerous and have been largely discussed in the literature.<sup>1</sup> Let us recall that these descriptions are well suited, especially when the modal density is high. The second hypothesis usually introduced is the diffuse-field assumption. Energy inside the system is uniformly and isotropically distributed. This crude simplification is surprisingly as much adapted to most current cases as their geometry is complex. In fact, the theoretical study of conditions that lead to a diffuse field is done by the mathematical theory of billiards.<sup>2,3</sup> This theory introduces the concept of mixing billiards for which two initially adjacent rays are arbitrarily distant in phase space after a sufficient time.<sup>4</sup> But it is well-known that the simplest billiards, such as rectangular or parallelepipedic ones, are not mixing! The more the geometry of the system is complex, the more the mixing property is assured. Applied to room acoustics, the diffuse-field concept results in a very simple relationship for time-reverberation: Sabine's formula, the success and popularity of which have not decreased for a century. More recently and in structural vibration, the so-called Statistical Energy Analysis (SEA)<sup>1</sup> has given rise to increasing interest. The diffuse-field assumption is constantly used and allows the evaluation of exchanged powers in terms of the vibrational energy of adjacent sub-systems. Sabine's formula and SEA make use of energy balance, and take the form of simple relationships for well-chosen variables; time-reverberation for the former and energies of sub-systems for the latter. The diffuse-field assumption leads to a major simplification; the

exact geometry of systems is of no importance. Only a few global parameters such as the areas and volumes of the systems matter.

Nevertheless, many authors have emphasized that the diffuse-field assumption is somewhat inadequate.<sup>5</sup> A perfect diffuse field cannot exist in the presence of absorbing walls because the isotropy imposes that energy flow should vanish everywhere, even in the vicinity of the walls. It is certainly the simplest approximation, whose efficiency results in useful relationships. However, it is sometimes necessary to account for anisotropy and inhomogeneous fields with an appropriate model. That case arises in the presence of highly absorbing walls, or rooms with one dimension much larger than the others, such as long corridors.<sup>6</sup>

For these unusual enclosures, the image-source method<sup>7</sup> and the ray-tracing technique<sup>8</sup> may be applied with efficiency. The diffuse-field assumption is no longer necessary, and the sound pressure level may be calculated for each observation point. On the other hand, the amount of calculation required is greater and, for instance, details of the geometry are taken into account. Many variations of the ray-tracing technique may be found in the literature: cones or rays, with or without phase, specular or diffuse reflection.<sup>9–11</sup> In this work, we are concerned with the approach which adopts the perfectly diffuse reflection law, namely Lambert's law. This law is valid for rough surfaces that cannot be described in a deterministic way, or for plane surfaces when a great number of rays impinge on them from all directions. Interference effects are neglected; that is to say, no phase is attached to rays or source magnitudes.

On this subject, one might also point out the method proposed by Kuttruff.<sup>12</sup> Under similar physical assumptions, a power balance at the boundary leads to an integral equation that determines the incident power. Carroll and Chien<sup>13</sup> solved this equation for spherical enclosures and showed how Sabine's formula should be modified. In a similar way, Miles<sup>14</sup> was interested in applying this method to rectangular enclosures and demonstrated that, after cutting-off the sound sources, and after a short instability period, "the field will

<sup>a)</sup>Electronic mail: lebot@mecasola.ec-lyon.fr

ultimately decay exponentially and at the same rate everywhere in the enclosure but it will not be diffuse during decay.’’ This confirms the time-reverberation concept, as well as correcting Sabine’s model. On the other hand, this method has been applied to structural vibrations in the steady state in Ref. 15. The coupling conditions between structural components involve reflection and transmission efficiencies whose mean values are also used in the calculation of coupling loss factors in SEA. All these studies emphasize the interest of this method concerning both the theoretical view and the numerical purpose.

The goal of this study is to compare results from geometrical acoustics with those of the integral method. To this end, two softwares have been used. One is the ray-tracing software RAYON designed by EDF; the second is the software CeReS especially built for the solving of the integral equation in vibroacoustic problems. Numerical simulations for some rooms are presented and predicted sound pressure level maps are compared.

## I. INTEGRAL EQUATION ON ENERGY

The aim of this method is to determine the energy density  $W$  and the energy flow  $\mathbf{I}$  resulting from sources in a domain  $\Omega$  with boundary  $\partial\Omega$ . To this purpose, the fields due to direct radiation have to be calculated first. They are, respectively, denoted by  $G(S, M)$  for the energy density at the observation point  $M$  induced by a unit excitation located at  $S$ , and  $\mathbf{H}(S, M)$  for the energy flow in similar conditions. We introduce specific notations  $G$  and  $\mathbf{H}$  for direct fields which will be frequently used in what follows, in order to avoid a confusion with complete fields  $W$  and  $\mathbf{I}$  which generally result from a superposition of many direct fields. Only steady-state equations are considered, since numerical simulations for transient-state problems have not been carried out. At first one has to write the energy-balance relationship to be verified,

$$\operatorname{div}_M \cdot \mathbf{H}(S, M) + mcG(S, M) = \delta_S(M), \quad (1)$$

where the first term is the net outgoing power per volume, the second term is the power density being dissipated ( $m$  is the usual atmospheric absorption factor and  $c$  the velocity of sound) and the right hand side is the injected power. As the fields  $G$  and  $\mathbf{H}$  propagate in an open space, they are related by a simple proportionality relationship,

$$\mathbf{H}(S, M) = cG(S, M)\mathbf{u}_{SM}, \quad (2)$$

where  $\mathbf{u}_{SM}$  is the unit vector from  $S$  toward  $M$ . The solutions of Eqs. (1), (2) are<sup>15</sup>

$$G(S, M) = \frac{1}{4\pi c} \frac{e^{-mSM}}{SM^2}, \quad (3)$$

$$\mathbf{H}(S, M) = \frac{1}{4\pi} \frac{e^{-mSM}}{SM^2} \mathbf{u}_{SM}, \quad (4)$$

where  $SM$  denotes the distance between  $S$  and  $M$ . Thus the energy of the direct field decreases for two reasons. First, the exponential term is due to the atmospheric absorption and, second, the geometric expansion imposes the attenuation fac-

tor  $1/SM^2$ ; that is, a decrease of 6 dB per doubling of distance.

The second step in developing the method is to find the complete fields  $W$  and  $\mathbf{I}$  in a domain  $\Omega$  with boundary  $\partial\Omega$ . Indeed they can be separated into direct fields previously determined, and reverberant fields caused by multiple reflections of energy impinging on the boundary. *All of these waves are assumed to be uncorrelated.* Many reasons enable to use such an assumption. For instance, the boundary may be irregular so that the exact position of the reflection is unknown. The phase of the reflected wave may then be considered as a random variable, and the results of the model are interpreted as the expected values of the actual variables. It should be remarked that such imperfection of boundary is most important, as the frequency increases, especially when the wavelength is comparable to the size of the irregularities. Another point of view is to consider that the exact positions of the excitation and observation points are imperfectly known. Furthermore, at high frequencies, a small displacement of one of these points leads to a drastically different response. Then a reasonable model should predict only the expected value of the response or, in other words, a local space-average of the response. A straightforward consequence of this hypothesis is that the energies of all waves may be summed without difficulties. This is a common fact in room acoustics, and explains why the use of energy quantities is so popular in high-frequency modeling. Referring to a classical integral representation, such as the Helmholtz–Kirchhoff formula, fields may be viewed as a superposition of spherical waves created by both actual sources located inside the domain  $\Omega$  and a source layer located on the boundary  $\partial\Omega$ . A direct transposition on energy fields leads to the following representation formulas,

$$W(M) = \int_{\Omega} \rho(S)G(S, M)dS + \int_{\partial\Omega} \sigma(P, \theta_P)G(P, M)dP, \quad (5)$$

$$\mathbf{I}(M) = \int_{\Omega} \rho(S)\mathbf{H}(S, M)dS + \int_{\partial\Omega} \sigma(P, \theta_P)\mathbf{H}(P, M)dP, \quad (6)$$

where  $\rho$  is the magnitude of the actual sources, obviously known, and  $\sigma$  denotes the magnitude of the secondary sources, yet to be determined. The directivity function of the secondary sources depends on the angle  $\theta_P$  between the outward normal at  $P$  and the emanating direction. We assume that *this directivity does not depend on the point  $P$* . In other words, and following Joyce,<sup>16</sup> this is a memoryless law, since the reflected directions are independent of the incident direction. A strong consequence of the second law of thermodynamics is that the only memoryless directivity function permitted is Lambert’s law,

$$\sigma(P, \theta_P) = \sigma(P)\cos \theta_P. \quad (7)$$

This is the law of perfectly diffuse reflection.

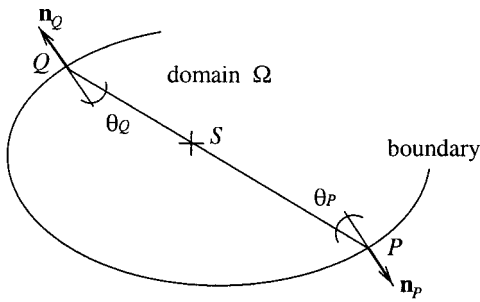


FIG. 1. Energy balance on the boundary  $\partial\Omega$ . The reflected power at  $P$  is the incident power stemming from actual sources  $S$  and other secondary sources  $Q$ , times the reflection coefficient  $1 - \alpha$ .

The third step is to develop an equation for secondary sources  $\sigma$ . This is achieved by applying the power balance at a point  $P$  on the boundary (see Fig. 1). The boundary dissipates a part of the incident energy; therefore, an absorption coefficient  $\alpha$ , defined as the ratio of reflected power to incident power, is then associated with it. The power balance is then

$$\mathcal{P}_{\text{refl}} = (1 - \alpha)\mathcal{P}_{\text{inc}}, \quad (8)$$

where the left hand side is the reflected power at point  $P$ , and  $\mathcal{P}_{\text{inc}}$  is the incident power of both the actual and secondary sources. The latter is the sum of all normal components of intensity vectors evaluated at  $P$ . Thus

$$\mathcal{P}_{\text{inc}} = \left[ \int_{\Omega} \rho(S)\mathbf{H}(S,P)dS + \int_{\partial\Omega} \sigma(Q)\cos\theta_Q\mathbf{H}(Q,P)dQ \right] \cdot \mathbf{n}_P, \quad (9)$$

where  $\mathbf{n}_P$  is the outward normal vector at point  $P$ . The reflected power can now be related to the source magnitude  $\sigma(P)$ . Consider a small hemisphere  $HS_\epsilon$  of radius  $\epsilon$  surrounding point  $P$ . The power flow crossing this hemisphere is

$$\mathcal{P}_{\text{refl}}^\epsilon = \sigma(P) \int_{HS_\epsilon} \frac{e^{-m\epsilon}}{4\pi\epsilon^2} \cos\theta_P dQ = \frac{\sigma(P)}{4} e^{-m\epsilon}. \quad (10)$$

The emitted power at point  $P$  is deduced by taking the limit for small  $\epsilon$ :

$$\mathcal{P}_{\text{refl}} = \lim_{\epsilon \rightarrow 0} \mathcal{P}_{\text{refl}}^\epsilon = \frac{\sigma(P)}{4}. \quad (11)$$

The power balance Eq. (8) can now be rewritten,

$$\frac{\sigma(P)}{4} = (1 - \alpha) \left[ \int_{\Omega} \rho(S)\mathbf{H}(S,P)dS + \int_{\partial\Omega} \sigma(Q)\cos\theta_Q\mathbf{H}(Q,P)dQ \right] \cdot \mathbf{n}_P. \quad (12)$$

This is a Fredholm integral equation of the second kind on the layer  $\sigma$ .

The software CeReS has been especially written to solve this equation in various circumstances. In this text,  $\Omega$  is an acoustical enclosure bounded by a surrounding surface  $\partial\Omega$ .

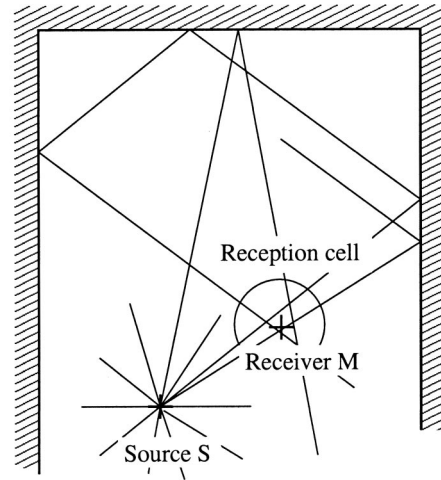


FIG. 2. Principle of the ray-tracing technique. Numerous rays are emitted from the source  $S$ , propagate in the room, are subjected to reflections on walls and, finally, arrive in the vicinity of the receiver point  $M$ . Energy at a point is evaluated by summing energies of all rays which cross the reception cell.

The CeReS software is able to treat other systems, such as assembled plates, for which the equations are slightly different from Eq. (12) (see Ref. 15). It seems that no attempt has previously been made to develop a software suitable for acoustical enclosures of arbitrary shape and size. The numerical simulations presented in Refs. 14, 12 are limited to parallelepipedic enclosures.

In the CeReS software, the boundary is assumed to be constructed with polyhedra of arbitrary shape and size, and the domain may be convex or not. The boundary is discretized into a sufficient number of triangles, and a collocation method with constant elements is implemented. Numerical integrals are evaluated with a standard Gaussian quadrature. Note that these integrals are regular, unlike the singular integrals involved in the classical boundary-element method, allowing a fast and accurate computation. The stability and the robustness of the algorithm depend on the existence and uniqueness of solutions for Eq. (12). This question is investigated in the following section. The theoretical formalism introduced to this end will turn out to be very useful for comparison with the ray-tracing method.

## II. EXISTENCE AND UNIQUENESS OF SOLUTION

In this section, we are interested in proving existence and uniqueness of solution for Eq. (12) in the special case of a convex domain  $\Omega$ . To this end, the boundary  $\partial\Omega$  is assumed to be compact. Equation (12) has no meaning if the outward normal does not exist. So, as a premise, we shall assume that such a normal vector exists almost everywhere. Now, let us write the integral operator involved in Eq. (12):

$$T: \sigma \mapsto \int_{\partial\Omega} \sigma(Q)K(Q,P)dQ, \quad (13)$$

where  $K(Q,P)$  is the kernel expressed as follows:

$$K(Q,P) = [1 - \alpha] \frac{e^{-mPQ}}{\pi P Q^2} \cos\theta_Q \cos\theta_P \geq 0 \quad (14)$$

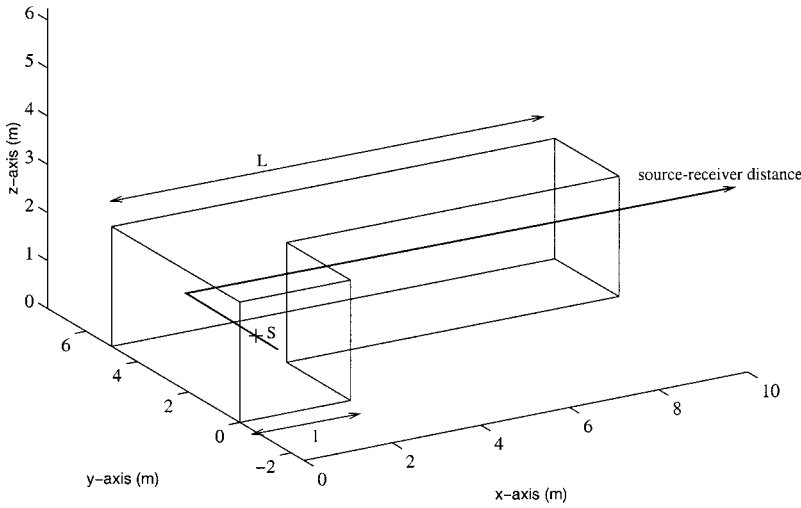


FIG. 3. View of the L-shaped room: the length ratio  $\lambda = L/l$  may vary. The source–receiver distance is taken along the thick line.

which is nonnegative by virtue of the convex assumption. Equation (12) can now be rewritten:

$$(Id - T)\sigma = g, \quad (15)$$

where

$$g(P) = [1 - \alpha] \int_{\partial\Omega} \rho(S) \frac{e^{-mSP}}{\pi SP^2} \cos \theta_P dS. \quad (16)$$

In practice, we are concerned with functions  $\rho(S)$  which are finite sums of Dirac functions representing point sources inside the domain (not on the boundary). For these functions  $\rho$ ,  $g$  is bounded over  $\partial\Omega$ . In the general case, we shall assume that function  $g$  is essentially bounded:  $g \in L^\infty(\partial\Omega)$ . A direct calculation gives

$$\int_{\partial\Omega} \frac{\cos \theta_P \cos \theta_Q}{\pi PQ^2} dQ = 1 \text{ for almost all } P \in \partial\Omega. \quad (17)$$

So the partial function  $Q \mapsto K(P, Q) \in L^1(\partial\Omega)$  is integrable over  $\partial\Omega$ ; its resulting integral  $P \mapsto \int_{\partial\Omega} K(P, Q) dQ \in L^\infty(\partial\Omega)$ ; the operator  $T$  maps the set  $L^\infty(\partial\Omega)$  of all essentially bounded functions into itself. And the following inequality:

$$\|T\sigma\|_\infty \leq \left\| \int_{\partial\Omega} K dQ \right\|_\infty \|\sigma\|_\infty \quad (18)$$

shows that  $T$  is a continuous operator whose norm is

$$\|T\| = \left\| \int_{\partial\Omega} K dQ \right\|_\infty \leq \sup_{\partial\Omega} (1 - \alpha). \quad (19)$$

For equality, check with  $\sigma = 1$ . Whenever  $\inf_{\partial\Omega} \alpha > 0$ , i.e., all the boundary is absorbing, the norm of the operator is less than one ( $\|T\| < 1$ ) and, following a well-known result valid for all Banach algebra, and, in particular, the Banach algebra  $L(L^\infty(\partial\Omega))$  of all continuous linear maps from  $L^\infty(\partial\Omega)$  into itself, the operator  $Id - T$  is invertible, so that Eq. (12) has a unique solution which can be written  $\sigma = (Id - T)^{-1}g \in L^\infty(\partial\Omega)$ .

### III. A REVIEW OF THE RAY-TRACING TECHNIQUE

The ray-tracing technique is of considerable interest for room-acoustic studies. Numerous softwares are available which attest to the industrial efficiency of such an approach. There are several approaches for the ray-tracing technique but, for the sake of brevity, we just describe the one adopted in the software RAYON2.1 of EDF (France)<sup>11,17</sup> that we used for the numerical simulations presented in this paper.

The basis of the method is as follows (see Fig. 2): A great number  $N$  of rays start from each sound source with power magnitude  $\rho$  in any direction. For instance, when sources are isotropic, the number of rays in a specific direction depends only on the solid angle, all rays having the same initial energy  $\epsilon(0) = \rho/cN$ . Rays propagate in straight lines and lose energy because of the sound absorption. After a distance  $x$ , the energy of the rays is  $\epsilon(x) = \rho e^{-mx}/cN$ . Rays reflect from surfaces they encounter. At each reflection, they lose a part  $\alpha$  of the incident energy so that, after  $n$  reflections and a total distance  $x$ , the residual energy is:  $\epsilon(x) = \rho e^{-mx} \prod_{i=1}^n (1 - \alpha_i)/cN$ . In RAYON, reflections may be specular or diffuse. In the first case, reflected angle is equal to incident angle whereas, in the second case, reflected direction is a probabilistic variable following the cosine law of Lambert. For the sake of consistency with the integral method of Sec. I, all numerical tests done with RAYON2.1 in the next section adopt Lambert's law of diffuse reflection.

One can finally calculate the energy at any observation point  $M$  inside the domain. Interference effects are not taken into account in the ray-tracing technique since multiple reflections of rays tend to uncorrelate the acoustic field. Thus energy at any spatial position is merely obtained by summing the energies of all rays reaching this location. Indeed, the probability for a ray to encounter the point is null. This difficulty is avoided in RAYON by introducing the notion of reception cells. These are spheres surrounding observation points. Energy density at any observation point is the energy contained in the reception cell—that is, the sum of energies of rays crossing the cell—divided by the sphere volume.

Rays are stopped when their energies become negligible or after a specified number of reflections. In both cases, re-

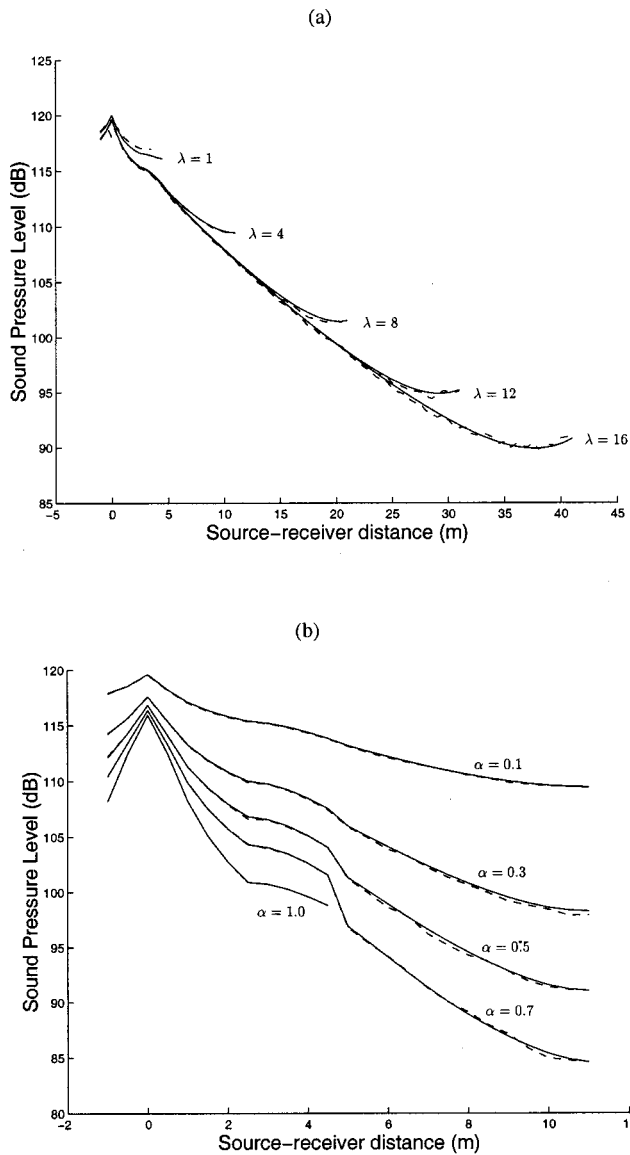


FIG. 4. Sound pressure level in a L-shaped room: comparison of sound pressure level ( $L_p$ -dB) from the ray-tracing technique (---) and from the collocation method (—) as a function of the source-receiver distance along the thick line crossing the room (see Fig. 3). (a) SPL for different values of  $\lambda$  with a uniform absorption factor  $\alpha=0.1$ . (b) SPL for different values of  $\alpha$  for  $\lambda=4$ .

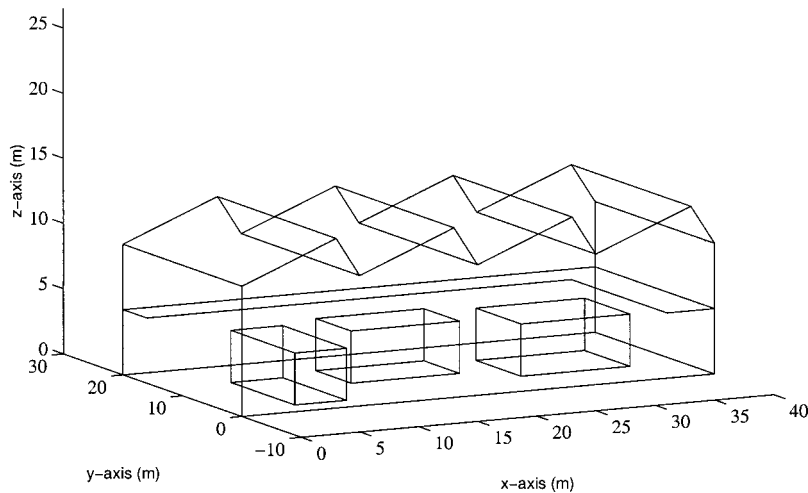


FIG. 5. View of the factory: ground, first floor and obstacles are located inside.

sidual energy is considered to be diffuse and is equally distributed over the whole domain.

#### IV. NUMERICAL SIMULATIONS

We have systematically compared both codes for numerous examples. Two different rooms with diffuse reflection are presented in this section. The first example is intended to examine the effect of varying shape, from a parallelepiped to a long corridor, and varying absorbing factors, from perfectly reflecting walls to totally absorbing walls. The second example is intended to demonstrate the applicability of the collocation method to more realistic rooms with complex shape and obstacles and floors contained inside. Our purpose is limited to the comparison of the two methods, and thus no experimental results are presented.

The first example is an L-shaped room with absorbing walls. Width and height are equal to  $l=2.5$  m, whereas the length  $L$  may vary. The nondimensional parameter  $\lambda=L/l$  characterizes the shape of the enclosure. Its value starts from 1 for a parallelepipedic room and increases to 16 for a long corridor. The source is located in the corner of the room at position  $x=1.25$  m,  $y=1.25$  m,  $z=1.7$  m (see Fig. 3). The response is evaluated along a horizontal line centered inside the room. All of these features are shown in Fig. 3. The atmospheric absorption is  $m=0.0007$   $\text{m}^{-1}$  which is a typical value at 1000 Hz. The calculation with the RAYON software was performed with 64 000 rays, which may be reflected up to 100 times. Their residual energy is 0.01% of the initial energy. The calculation with CeReS software was performed with a mesh of triangles with areas of  $0.4$   $\text{m}^2$ . Results of the comparison are shown in Fig. 4. The top graph compares the sound pressure level,  $L_p$ , for different values of the ratio  $\lambda$ , with a uniform absorption factor  $\alpha=0.1$ . The second graph compares the sound pressure level,  $L_p$ , for different absorption factors, with  $\lambda=4$ . In the case of totally absorbing walls,  $\alpha=1$ , the acoustical energy cannot reach any point in the right part of the room since it vanishes at the first reflection. All these comparisons show a good agreement between the ray-tracing technique and the integral method.

The second example is a hypothetical factory with sound-absorbing walls, floors and obstacles. The geometry is shown in Fig. 5. This is a nonconvex room with volume  $V$

TABLE I. Absorption factors for the factory. Obstacles are numbered 1 to 3 from left to right in Fig. 5.

Surface	Absorption factor $\alpha$	Area (m <sup>2</sup> )
ground floor	0.05	627.4
first floor (both sides)	0.1	448
ceiling	0.05	972
front and back walls $x=0$ m, $x=40$ m	0.02	400
lateral walls $y=0$ m, $y=20$ m	0.02	460
surfaces of obstacle 1	0.2	169.1
surfaces of obstacle 2	0.3	176.8
surfaces of obstacle 3	0.25	204.3

$=8509$  m<sup>3</sup> and total surface area  $S=2305$  m<sup>2</sup>. The absorption factors are summarized in Table I. Floors, ceiling and walls are highly reflective; the absorption is essentially due to obstacles inside the factory. The area-averaged absorption coefficient is  $\bar{\alpha}=0.12$ . Thus the room constant is  $R=\bar{\alpha}S/(1$

$-\bar{\alpha})=319$  m<sup>2</sup>. The atmospheric absorption is  $m=0.0007$  m<sup>-1</sup>. The critical radius is  $r_c=(R/16\pi)^{1/2}=2.5$  m; that gives an indication of how far from the source the direct field is predominant. Three sources are located in the factory. Their positions are:  $x=5$  m,  $y=5$  m,  $z=1$  m for source 1;  $x=20$  m,  $y=5$  m,  $z=1$  m for source 2; and  $x=35$  m,  $y=15$  m,  $z=1$  m for source 3. The power levels of these sources are 120 dB (1 W). The calculation with RAYON is performed with 64 000 rays which may be reflected up to 100 times. Their residual energy is 1% of the initial energy. The calculation with CeReS is performed with a mesh of 586 triangles for boundary elements. Results are shown in Figs. 6, 7 and 8 with, respectively, one, two and three sources active. In each case, the top map is the sound pressure level ( $L_p$ -dB) computed with RAYON on a plane 2 m above the ground floor, and the bottom map is computed with CeReS on the same plane. The additional graphs on the right com-

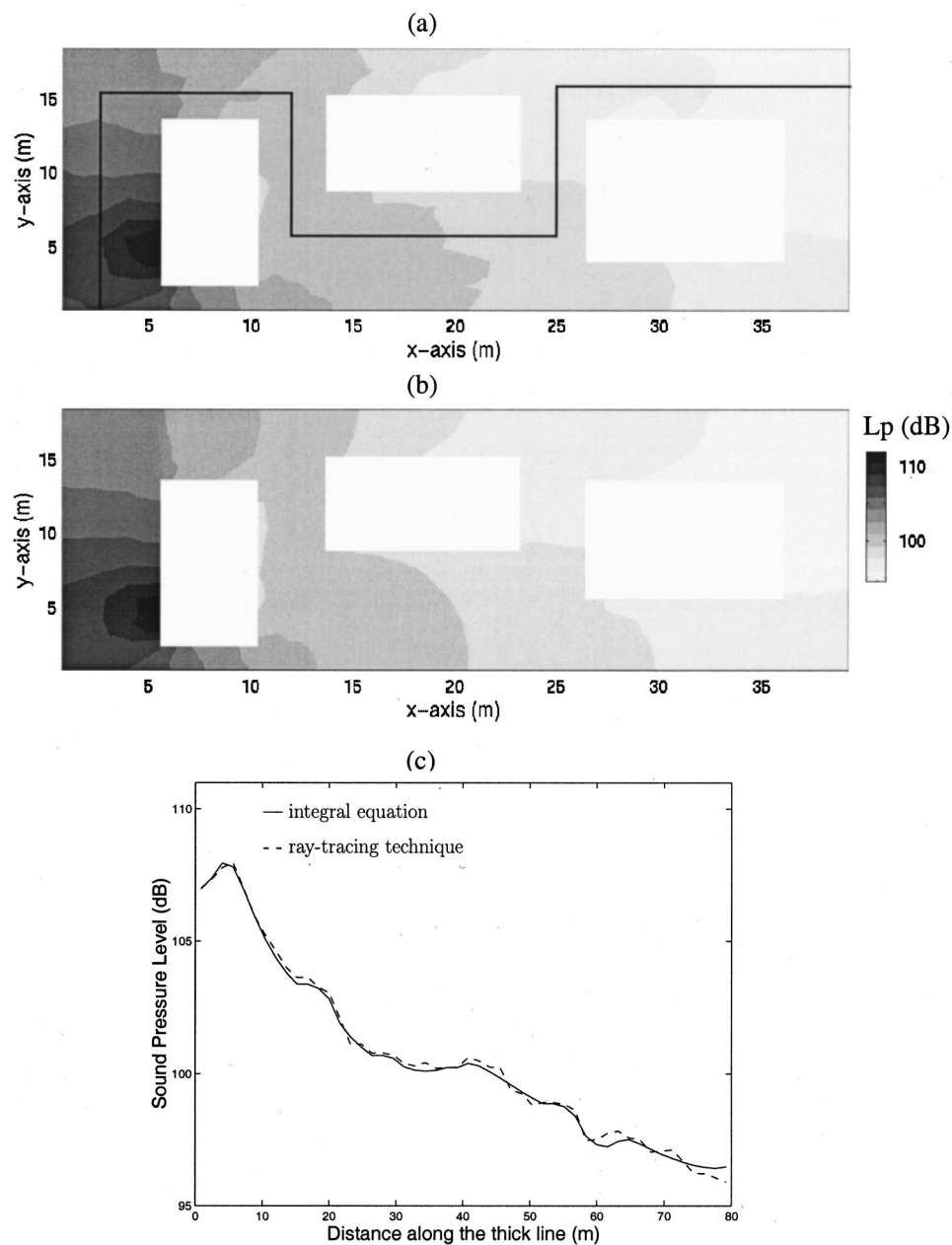


FIG. 6. Noise in a factory: comparison of sound pressure level ( $L_p$ ) by (a) the ray-tracing technique, and by (b) the integral formulation on a horizontal receiver plane 2 m above the floor. (c) Direct comparison of SPL along the thick line. One source is active.

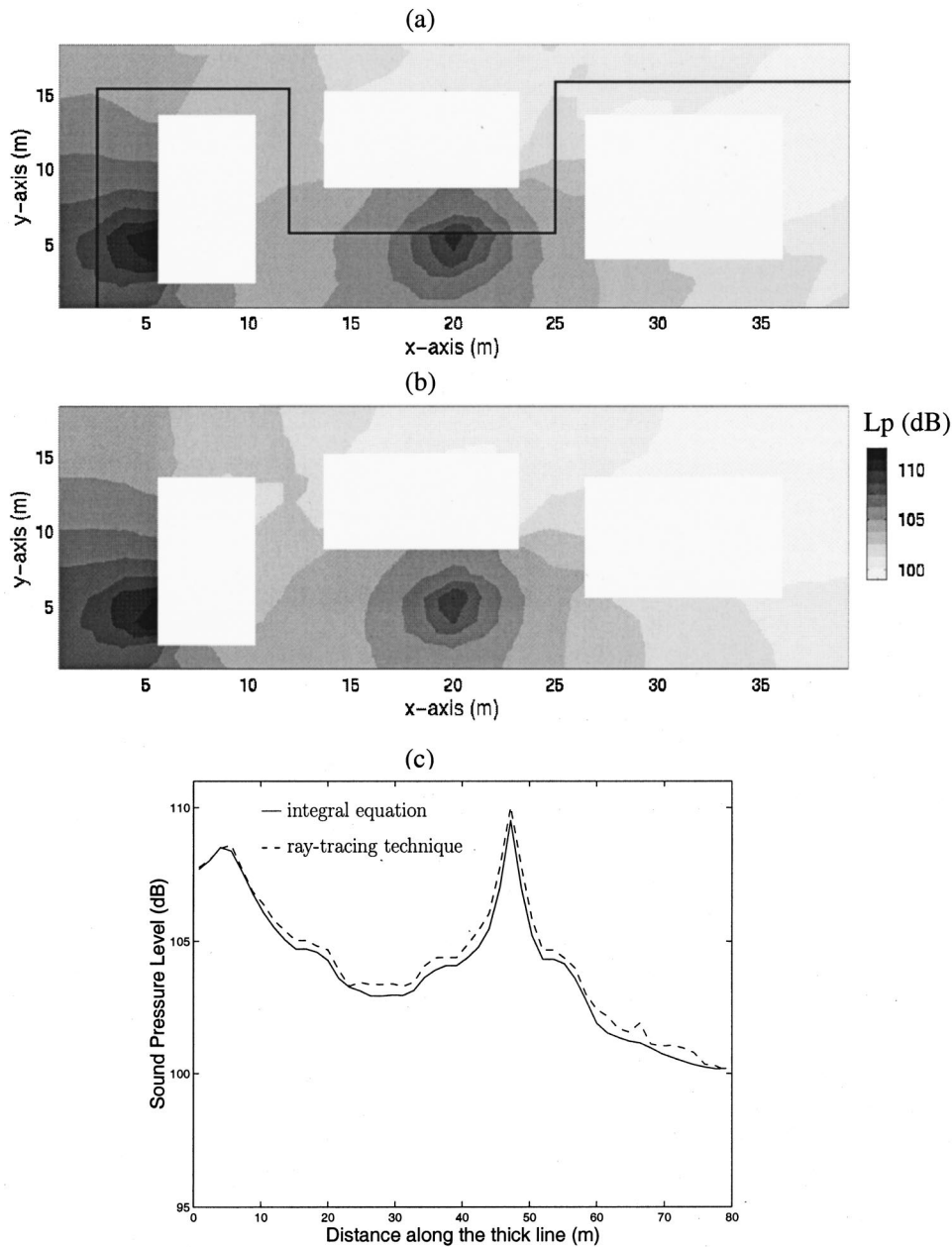


FIG. 7. Noise in a factory: same conditions as Fig. 6 with two sources active.

pare directly the SPL along the axis of the thick line visible on the maps.

Results of these examples highlight an excellent agreement between the two algorithms. Although the numerical schemes are quite different—Monte Carlo for RAYON and collocation method for CeReS—the physical assumptions are similar: interference effects neglected and diffuse reflection on walls. These numerical simulations suggest that the two methods are equivalent. The next section proposes a formal proof for this equivalence.

## V. EQUIVALENCE OF THE METHODS

To prove that the ray-tracing technique is close to the integral method, consider the operator  $T$  defined in Sec. II. We saw that its norm is less than one (in the mathematical meaning of norm of bounded linear mappings of Banach spaces; see for instance Ref. 18, Chapter 4) and we deduced the existence and the uniqueness of the solution for Eq. (12).

However, the fact that  $\|T\| < 1$  leads to an additional result. The operator  $(Id - T)^{-1}$  can be developed into a Neumann series:

$$(Id - T)^{-1} = Id + T + T^2 + \dots + T^n + \dots \in L(L^\infty(\partial\Omega)). \quad (20)$$

Thus

$$\sigma = g + Tg + T^2g + \dots + T^ng + \dots \in L^\infty(\partial\Omega). \quad (21)$$

At each point  $P$ ,  $\sigma$  is the reflected power. It is the sum of the reflected part of the incident power of the direct field  $g$  and those of the powers after one reflection, two reflections, and so on. Finally, the energy inside the domain at  $M$  is

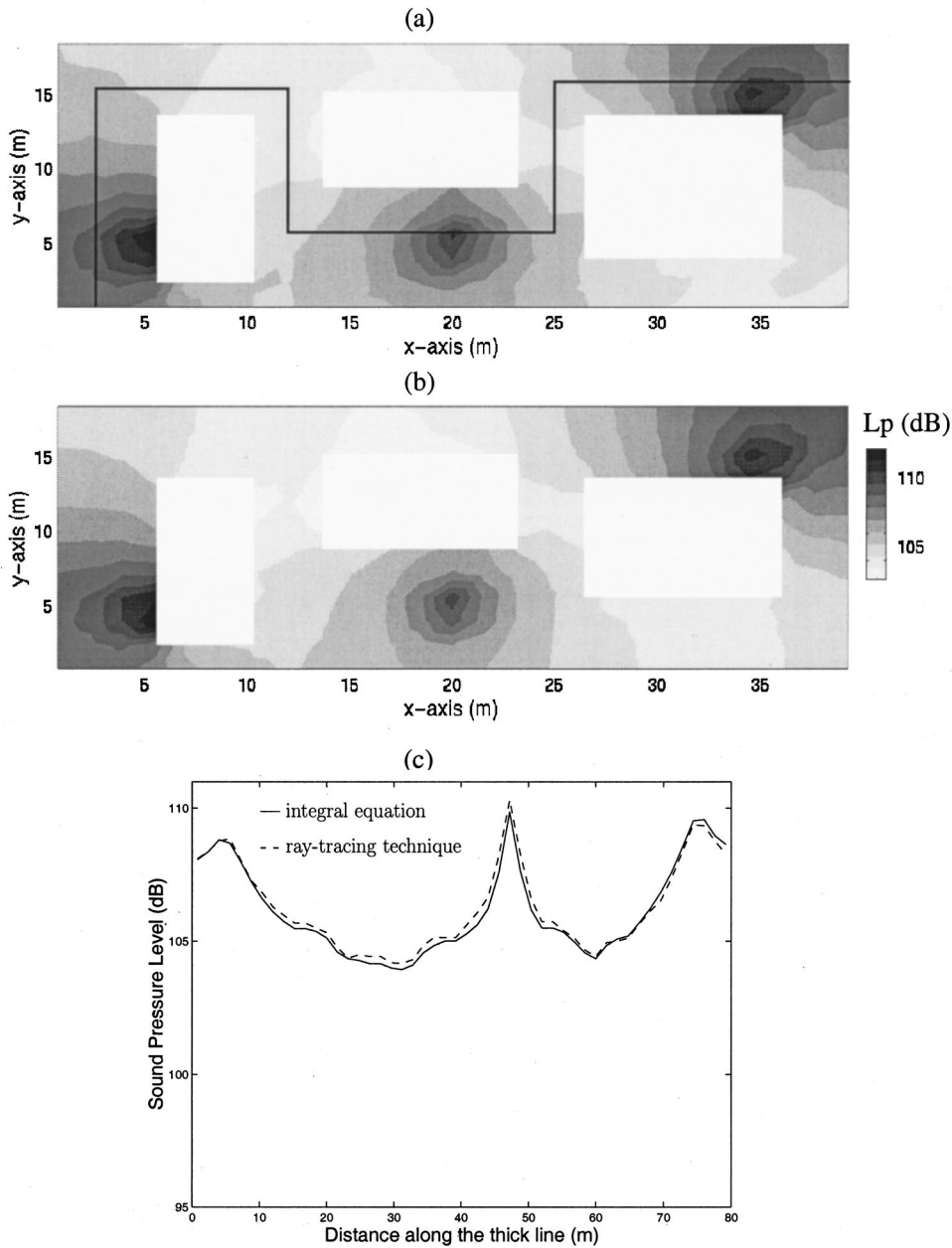


FIG. 8. Noise in a factory: same conditions as Fig. 6 with three sources active.

$$\begin{aligned}
 W(M) = & \int_{\Omega} \rho(S)G(S,M)dS + \int_{\Omega} g \cos \theta_P G(P,M)dP \\
 & + \int_{\Omega} Tg \cos \theta_P G(P,M)dP + \dots \\
 & + \int_{\Omega} T^n g \cos \theta_P G(P,M)dP + \dots, \quad (22)
 \end{aligned}$$

and we find that the energy at  $M$  is the sum of the energy of the direct field and the energies carried by rays which have been reflected once, twice, and so on. It is clear from this development how the ray algorithm is hidden in the integral equation (12). The ray-tracing technique is seen to be a numerical evaluation by the Monte Carlo method of the above integrals Eq. (22).

## VI. CONCLUSION

In this study, we have compared results of two methods for calculating acoustic pressure fields in rooms. The first is the well-known ray-tracing technique; the second is based on an integral equation obtained by balancing powers at any points of the boundary.

The methods were implemented into softwares called RAYON and CeReS that can solve all cases of acoustic enclosures limited by arbitrary polyhedra. The numerical examples that we treated show that the two methods give identical results. Actually, both methods are based on the same physical assumptions, which are energy superposition and diffuse reflection.

The formal proof of the equivalence of the two methods stems from the Neumann development of the integral operator. This has been possible because the norm of the operator

is less than one. The ray-tracing technique is seen to be a numerical method for the computation of the integrals Eq. (22) by the Monte Carlo procedure, whereas the CeReS software uses a collocation method for the evaluation of the same integrals.

It is not clear whether the numerical method has advantages over the other method. Computing times for the RAYON and CeReS softwares are similar. The ray-tracing technique is simpler to implement. In any case, this method is well established, and highly optimized algorithms are available.

The advantages of the integral method are rather theoretical. The formulation is continuous, in contrast to the discrete description of the ray-tracing method. In addition, with the integral equation, we have the use of an equation that has a closed-form solution in contrast to the ray-tracing technique that only leads to numerical solutions. For instance, in Ref. 13, Carroll and Chien give a closed-form solution for the energy field inside a spherical enclosure. It would be very difficult to obtain such a result with the ray-tracing technique.

## ACKNOWLEDGMENTS

The authors gratefully acknowledge L. Ricol and E. Luzzato (EDF) for their advice, numerical computations with RAYON, and financial support.

<sup>1</sup>R. H. Lyon, *Statistical Energy Analysis of Dynamical Systems: Theory and Application* (MIT Press, Cambridge, MA, 1975).

<sup>2</sup>M. Berger, "La mathématique du billard," *Pour la Science* **163**, 76–85 (1991).

<sup>3</sup>V. I. Arnold and A. Avez, *Problèmes Ergodiques de la Mécanique Classique* (Gauthier-Villars, 1967).

<sup>4</sup>J. D. Polack, "Playing billiards in the concert hall: The mathematical foundations of geometrical acoustics," *Appl. Acoust.* **38**, 235–244 (1993).

<sup>5</sup>H. Kuttruff, *Room Acoustics*, 3rd ed. (Elsevier, New York, 1991), p. 102.

<sup>6</sup>J. Kang, "Reverberation in rectangular long enclosures with geometrically reflecting boundaries," *Acust. Acta Acust.* **82**, 509–516 (1996).

<sup>7</sup>J. Borish, "Extension of the image model to arbitrary polyhedra," *J. Acoust. Soc. Am.* **75**, 1827–1836 (1984).

<sup>8</sup>A. Krostad, S. Strom, and S. Sorsdal, "Calculating of the acoustical room response by the use of a ray-tracing technique," *J. Sound Vib.* **8**, 118–125 (1968).

<sup>9</sup>J. L. Barbry, "Techniques des images et des rayons (locaux vides)," *Publication de l'Institut National de Recherche et de Sécurité*, 51 (1984).

<sup>10</sup>D. Maercke and J. Martin, "The prediction of echograms and impulse responses within the epidaure software," *Appl. Acoust.* **38**, 93–114 (1993).

<sup>11</sup>L. Ricol and F. Junker, "A ray tracing software: RAYON2.0," in *Euro-Noise 95, Lyon France*, pp. 49–54, 1995.

<sup>12</sup>H. Kuttruff, "A simple iteration scheme for the computation of decay constants in enclosures with diffusely reflecting boundaries," *J. Acoust. Soc. Am.* **98**, 288–293 (1995).

<sup>13</sup>M. M. Carroll and C. F. Chien, "Decay of reverberent sound in a spherical enclosure," *J. Acoust. Soc. Am.* **62**, 1442–1446 (1977).

<sup>14</sup>R. N. Miles, "Sound field in a rectangular enclosure with diffusely reflecting boundaries," *J. Sound Vib.* **92**, 203–226 (1984).

<sup>15</sup>A. Le Bot, "A vibroacoustic model for high frequency analysis," *J. Sound Vib.* **211**, 537–654 (1998).

<sup>16</sup>W. B. Joyce, "Sabine's reverberation time and ergodic auditoriums," *J. Acoust. Soc. Am.* **58**, 643–655 (1975).

<sup>17</sup>E. Luzzato and D. Taillifet, "Les modèles de l'acoustique prévisionnelle intérieure," *EDF-Bulletin de la Direction des Études et Recherches*, 1 Série C 5–37 (1988).

<sup>18</sup>W. Rudin, *Functional Analysis* (McGraw-Hill, New York, 1991).